submitted to *BSSA*

The aftershock sequence of the Mw 6.3 2010 Rigan earthquake in southeast Iran: further evidence of a hidden fault in the southern Lut Block.

Reza Mansouri[1], Alessia Maggi[2], and Jean-Paul Montagner[3]

[1] *Institute of Geophysics, University of Tehran, Tehran, Iran*

[2] *Institut de Physique du Globe de Strasbourg, CNRS et Université de Strasbourg (EOST), France*

[3] *Institut de Physique du Globe de Paris, Paris, France*

19 January 2015

Electronic supplement: The electronic supplement to this paper contains a detailed description of the time-reversal (migration) algorithm we used for our preliminary detection and location of the aftershocks of the Rigan earthquake. It also contains final locations for 46 well-located aftershocks.

SUMMARY

The Mw 6.3 20 December 2010 earthquake near Rigan in southeastern Iran occurred on a previously unknown active fault in the southern Lut block. Its position was inferred by Walker et al. (2013) using InSAR and the analysis of aftershocks recorded by the two permanent seismological networks in Iran. In this paper we analyse previously unavailable data from six temporary stations deployed immediately after the 2010 Rigan earthquake. We locate the aftershock sequence using two techniques: a time-reversal method of our own, derived from the Waveloc algorithm of Langet et al. (2014), and the NonLinLoc algorithm of Lomax et al. (2000). We detect over 3900 events over the 7-day period of the deployment, 46 of which we consider to be well constrained. Our locations lie on a northeast-southwest trend that corroborates the inferred fault location, and provides further evidence of the presence of this hidden fault in the southern Lut block. The occurrence of hidden faults in this tectonically active region suggests that a re-evaluation of local and regional seismic hazard may be necessary.

Key words: seismology – earthquake location – migration

INTRODUCTION

The Iran plateau is trapped between the Arabian plate to the South and the Eurasian plate to the North. It is composed of a number of micro-continental blocks and ocean-floor basins separated by major deformation zones (e.g. Berberian 1981). The Lut Block is located in central-eastern Iran, extends about 900 km North to South and 200 km East to West (Fig. 1a), and has generally been considered non-deforming. It is bounded in the North by the Doruneh Fault, in the South by the Jazmourian Depression, in the East by the Nehbandan fault system and in the West by the Nayband Fault and the Gowk Fault system (Hessami and Jamali 2006).

On 20 December 2010, a moderate but destructive earthquake of Mw 6.3 struck southeastern Iran near Rigan, a village in near the southern tip of the Lut block (Fig. 1b). This earthquake caused extensive damage to many buildings in the region (e.g. Walker et al. 2013). It was preceded by a small (ML 3.7) foreshock and followed by 126 aftershocks, as detected by the IRSC - Iranian Seismological Center. Although these aftershocks were relatively small (ML $<$ 4.6), many of them were recorded at local and regional distances. Another moderate but non-destructive earthquake of Mw 6.2 struck the nearby region on 27 January 2011 (Fig. 1b). These two events occurred in a region that was not known to have any active faults. Unless otherwise specified, all magnitudes in this paper are those calculated by the IRSC, the Iranian Seismological Center.

Both the 2010 and the 2011 Rigan earthquakes were studied in detail by Walker et al. (2013). Using surface displacements from SAR interferometry and teleseismic body waveform modelling, they inferred that the 2010 event occurred with a right-lateral strike-slip motion on a previously unknown near-vertical fault with strike $\sim$N210°, and that the 2011 event occurred with a left-lateral strike-slip motion on another previously unknown near-vertical fault with strike $\sim$N310° (see their proposed fault traces in Fig. 1b). Although the authors successfully mapped a series of minor cracks and en-echelon fissures that had appeared after these earthquakes, neither event produced a clear surface trace. Walker et al. (2013) also relocated the aftershock sequences of both events using data from the two main permanent seismic networks in Iran, operated respectively by the International Institute for Seismology and Earthquake Engineering (IIEES), and the Iran Seismological Center (IRSC). These relocations are broadly consistent with the positions of the faults inferred from their InSAR analysis, but do not show a strong alignment. A previous aftershock analysis performed by Maleki and co-authors using only IRSC permanent stations produced two broad clouds of locations (see Fig. 8 in Maleki et al. 2012).

Currently, the main constraints on the position and orientation of the faults for the 2010 and 2011 Rigan events are those obtained using InSAR analysis by Walker et al.

(2013). Seismological constraints on their aftershock sequences, obtained using one or both permanent seismological networks in Iran, are still relatively poor (Maleki et al. 2012; Walker et al. 2013). In this paper, we present a much clearer seismological picture of the aftershock sequence of the 2010 Rigan earthquake, thanks to the deployment of a temporary local seismic network in the region shortly after the event. Our aftershock locations strongly corroborate the presence of the hidden fault inferred by Walker et al. (2013).

METHODS

The data used in this study consist of continuous waveforms recorded by six temporary stations deployed by the IRSC in the Rigan region (Fig. 1b) shortly after the 20 December 2010 Mw6.3 earthquake. The stations recorded a significant number of aftershocks and micro-seismic events. In this paper we analyse data from the 7-day period from 29 December 2010 to 4 January 2011. The waveforms recorded on 3 January 2011 are shown in Fig. 2 to illustrate data quality.

We analyzed the seismicity recorded by this temporary deployment using two techniques. The first is a time-reversal (TR) or migration method inspired by the work of Withers et al. (1999), Maggi and Michelini (2010) and Langet et al. (2014) at local and regional scales and Larmat et al. (2006) at the global scale. The second technique is the NonLinLoc location method of Lomax et al. (2000), which we applied on a subset of the aftershocks detected by our time-reversal method.

Our TR method is a 3-step procedure: the first step consists in simplifying the observed waveforms by computing a kurtosis-based characteristic function, which has the property of producing high peaks at the first P-wave arrival times; the second step consists in convolving these characteristic functions with Greens functions calculated through a regional Earth model and then stacking them appropriately on a 3D grid of test-hypocenters; the third step consists in determining the local space-time maxima in the resulting 4-D stacked volume in order to detect and approximately locate the seismic events. Our first and third steps are derived from the Waveloc algorithm of Langet et al. (2014); our second step is a re-implementation of the convolution algorithm of Withers et al. (1999) and Maggi and Michelini (2010). The strengths of methods like ours are their high detection rate and the fact that they do not require phase association (a step required in traditional earthquake location which becomes complex for dense aftershock sequences or seismic swarms). Their major weakness is the poor depth resolution due to the exclusive use of P-wave arrivals. A more detailed description of the method, including the synthetic tests we used to determine the best parameters to use for the Rigan dataset, is available in the electronic supplement to this article.

In applying our method to the Rigan dataset, we band-pass filtered the raw data between 1Hz and 10Hz, used a 3-second window for kurtosis processing and a regular 3D grid with 2km spacing for the stack grid. We supposed a 1D crustal seismic velocity model based on the CRUST2.0 (Bassin et al. 2000) parameters for the Rigan region in order to compute the Greens functions (Table 1). A zero-noise synthetic resolution test for the Rigan network is shown in Fig. 3, and indicates that shallow events ($\sim$5 km depth) should be located with at worst a 10 km uncertainty, while deeper events ($\sim$15 km depth) should be located with at worst a 15 km uncertainty.

The first pass of our TR algorithm on the Rigan dataset detected more than 3900 events over the 7-day period. In the results section, we limit our discussion to the well-constrained events, which we define as being those located using all 6 temporary stations of the Rigan network with an azimuthal gap less than 270° and a horizontal uncertainty of less than 20 km. Fewer than 50 events satisfied all these conditions.

As our algorithm is based on a non-adaptive grid of possible hypocenter locations, the accuracy of the locations (even the well-constrained ones) can never be better than the grid-spacing. Other factors may further increase the uncertainty of our locations. Firstly the kurtosis characteristic function is often unable to pin-point the exact onset time: although an improvement over the STA/LTA method, the kurtosis method remains an automated algorithm and as such is unequal to an expert manual picker. Secondly our method uses only the P-wave arrival information to perform the migration and thus has a poor depth resolution. Thirdly the velocity model we use may be inappropriate: CRUST2.0 is a 2°x2° approximation of crustal structure on a global scale, and cannot represent the variability of seismic velocity in our relatively small study area.

In order to improve the locations of these well-constrained events, we manually picked their P-wave arrivals on the 6 stations of the temporary network, then located them using the NonLinLoc (NLL) algorithm of Lomax et al. (2000). NLL is a probabilistic global-search algorithm which has been applied in a number of prior studies including Lomax (2005). In contrast to linearized methods where the hypocenter location of an event is defined by a single point and its associated error, in NLL the hypocenter location is determined by a set of points resulting from the posterior probability density function. We have chosen to use only P-wave arrivals - because only very few S-wave arrivals were clearly recorded on all stations - and the same velocity model as that used for the TR location (Table 1). We shall not be able to discuss the effect of the velocity model on the locations by comparing the two sets of locations.

RESULTS AND DISCUSSION

The locations of the 46 well-constrained events detected and located by our TR method are shown as red symbols in Fig. 4a. They are mostly aligned along a northeast-southwest trend, and their local magnitudes range between 2.1 and 4.6. Over the same 7-day period, IRSC only located 15 events, shown as white symbols in Fig. 4a. Fourteen of the IRSC events are included within our well-constrained events.

The low number of events detected by IRSC is probably due to sparse station coverage (they only use permanent stations for their locations) and the large distances of the permanent stations to the Rigan region (the closest is 222 km away). Comparison between the IRSC locations and our own indicates a systematic geographical bias of 23.5 km along an azimuth of 180°, with the IRSC locations systematically to the north of our locations. The distance between the centers of the two clusters of events is approximately 16 km. This bias is probably due to a combination of sparse station coverage, large event-station distances and high azimuthal gaps (the azimuth gaps for these events range from 121° to 294° for the IRSC permanent network and from 122° to 160° for our Rigan network).

We have used the geographical bias measured on the common aftershocks to shift the original IRSC locations for the 2010 and 2011 Rigan events. The original IRSC locations, our shifted locations and the preferred locations of Walker et al. (2013) are shown in Table 2 and in Fig. 5a. The shifted IRSC locations align much better with the aftershock locations than the original ones, and are also much closer to the Walker et al. location. Both these observations give us reasonable confidence in our estimate of the geographical bias in the IRSC locations. Improving the IRSC permanent locations in this region would require installation of more permanent stations in the eastern Lut block, and/or collaboration with the countries bordering Iran to the East, i.e. Afghanistan and Pakistan. As the current geopolitical situation in the region may render such installations or collaborations difficult for the time being, we suggest that correction of the geographical bias as we have done in this study might be an appropriate temporary solution for the study of future seismicity in this part of the Lut block.

The NLL locations of our 46 well-constrained aftershocks are shown in Fig. 5, and are listed in Table S3, available in the electronic supplement to this article. The maximum uncertainty of these locations is 10 km, and the maximum depth uncertainty is 3 km. The reduction in horizontal uncertainties of these locations with respect to those obtained with our TR method is due to a combination of more precise (manual) picking and the oct-tree adaptive grid-search process implemented by NLL. All but three events are clearly aligned on a northeast-southwest trend and their depths are mostly limited to the upper 10km of crust. The linear trend is much clearer in Fig. 5a than for the Walker et al. (2013) locations (see Fig. 1b), and provides further evidence of the existence of the hidden fault. Our linear trend seems to be located approximately 3 km to the southeast of the fault position inferred by Walker et al. (2013) for the 2010 event, indicating there may still be a small residual geographical bias in our locations. Four aftershocks of the 2010 event seem to lie along the fault that Walker et al. (2013) inferred for the 2011 event, which leads us to speculate that they might represent its foreshocks.

CONCLUSION

We have analyzed the aftershock sequence of the 20 December 2010 Mw 6.3 Rigan earthquake in southeastern Iran using data from the IRSC deployment of six temporary stations in the region immediately after the earthquake. We have used two different methods to locate the events: a time-reversal method of our own, derived from the Waveloc algorithm of Langet et al. (2014), and the NonLinLoc algorithm of Lomax et al. (2000). We have detected over 3900 events, 46 of which we consider to be well constrained (i.e. located by all six temporary stations). In this paper we have :

(i) corroborated the position and orientation of the fault of the 2010 Rigan event inferred from InSAR analysis by Walker et al. (2013);

(ii) found evidence for a systematic, magnitude-dependent geographical bias in the routine locations obtained by the IRSC in this region using only data from the permanent seismic stations.

After these two events, and the destructive event that struck Bam in 2003 (Talebian et al. 2004; Jackson et al. 2006), we can no longer consider this part of Iran to be free of deformation. The active faults that gave rise to these three events had not been identified prior to the events themselves, as they have little or no surface expression, and as the coverage of this region in permanent seismic stations is poor (the closest station is 220 km away). It is probable that better seismic monitoring of the region would bring to light a clearer picture of the active faults in this region, with implications both for the understanding of local and regional tectonics and the evaluation of seismic hazard.

Data and resources

The dataset used for the analysis was collected by the Iranian Seismological Center (IRSC). The stations were equipped with broad-band Trillium 40s sensors and Taurus digitizers configured with a sampling frequency of 100Hz. The Waveloc code cited in this paper is open-source, is released under the CeCILL license and can be downloaded from `http://amaggi.github.io/waveloc` (last accessed December 2014). Waveloc is written in Python, and was developed using the Enthought Python distribution under an academic license. The NonLinLoc package of Lomax et al. (2000) can be downloaded from `http://alomax.free.fr/nlloc` (last accessed December 2014). The synthetic seismograms used for the tests described in the electronic supplement were synthesized using the Computer Programs in Seismology package that can be downloaded from `http://www.eas.slu.edu/eqc/eqccps.html` (last accessed December 2014).

Acknowledgments

We would like to thank IRSC for providing the data from the temporary deployment in the Rigan region. The development of the Waveloc software was supported by the Network of European Research Infrastructures for Earthquake Risk Assessment and Mitigation (NERA, EC Grant Number 262330).

REFERENCES

Bassin, C., G. Laske, and G. Masters (2000). The current limits of resolution for surface wave tomography in North America, *EOS Trans. AGU*, **81**(F897).

Berberian, M. (1981). Active faulting and tectonics of Iran, in *Zagros Hindu Kush Himalaya Geodynamic Evoluion*, eds Gupta, H. K. and F. M. Delany, American Geophysical Union, Washington, D.C., doi: 10.1029/GD003p0033.

Hessami, K. and F. Jamali (2006). Explanatory notes to the map of major active faults of Iran, *Journal of Seismology and Earthquake Engineering*, **8**(1), 1–11.

Jackson, J., M. Bouchon, E. Fielding, G. Funning, M. Gorashi, D. Hatzfeld, H. Nazari, B. Parsons, K. Priestley, M. Talebian, M. Tatar, R. Walker, and T. Wright (2006). Seismotectonic, rupture-process, and earthquake-hazard aspects of the 2003 December 26 Bam, Iran, earthquake, *Geophysical Journal International*, **166**, 1270–1292.

Langet, N., A. Maggi, A. Michelini, and F. Brenguer (2014). Continuous kurtosis-based migration for seismic event detection and location, with application to Piton de la Fournaise volcano, La Réunion, *Bulletin of the Seismological Society of America*, **104**(1), 229–246.

Larmat, C., J. P. Montagner, M. Fink, Y. Capdeville, A. Tourin, and E. Clévédé (2006). Time-reversal imaging of seismic sources and application to the great Sumatra earthquake, *Geophysical Research Letters*, **33**(L19312), doi: 10.1029/2006GL026336.

Lomax, A. (2005). A re-analysis of the hypocentral location and related observations for the Great 1906 California Earthquake, *Bulletin of the Seismological Society of America*, **95**, 861–877.

Lomax, A., J. Virieux, P. Volant, and C. Berge (2000). Probabilistic earthquake location in 3d and layered models: Introduction of a Metropolis-Gibbs method and comparison with linear locations, in *Advances in Seismic Event Location*, pp. 101–134, eds Thurber, C. H. and N. Rabinowitz, Kulwer Academic.

Maggi, A. and A. Michelini (2010). Waveloc: An algorithm for the detection and location of seismic sources within large, continuous waveform data volumes: The case of the l'Aquila earthquake sequence, in *Geophysical Research Abstracts*, EGU, Vienna, Austria.

Maleki, V., Z. H. Shomali, and M. R. Hatami (2012). Relocation of the aftershocks of Mohamad Abad Rigan earthquake December 20, 2010, (MN=6.5) using a nonlinear method, *Iranian Journal of Geophysics*, **6**(4), 96–111.

Talebian, M., E. J. Fielding, G. J. Funning, M. Gorashi, J. Jackson, H. Nazari, B. Parsons, K. Priestley, P. A. Rosen, R. Walker, and T. J. Wright (2004). The 2003 Bam (Iran) earthquake: Rupture of a blind strike-slip fault, *Geophysical Research Letters*, **31**(L11611), doi: 10.1029/2004GL020058.

Walker, R. T., E. A. Bergman, J. R. Elliott, E. J. Fielding, A. R. Ghods, M. Gorashi, J. Jackson, H. Nazari, M. Nemati, B. Oveisi, M. Talebian, and R. J. Walters (2013). The 2010-2011 South Rigan (Baluchestan) earthquake sequence and its implications for distributed deformation and earthquake hazard in southeast Iran, *Geophysical Journal International*, **193**, 349–374.

Withers, M., R. Aster, and C. Young (1999). An automated local and regional seismic event detection and location system using waveform correlation, *Bulletin of the Seismological Society of America*, **89**(3), 657–669.

Table 1. Velocity model for the Rigan region.

Depth to top of layer (km)	V_P (km/s)	V_S (km/s)	Density (g/cc)
0.0	2.5	1.2	2.1
0.5	6.1	3.5	2.7
14.0	6.3	3.6	2.8
28.0	7.2	4.0	3.1
38.0	8.0	4.6	2.3

Table 2. Locations of the 20 December 2010 Rigan earthquake.

Location	Latitude	Longitude	Depth
IRSC	28.44	59.15	13.3
IRSC bias removed	28.23	59.15	13.3
Walker et al. (2013)	28.33	59.19	10
Global CMT	28.11	59.11	14.8

LIST OF FIGURES

5 Locations of the 46 well-constrained events obtained using manual picking and NLL. (a) Map of the 46 aftershock epicenters (white circles), showing also the epicenters (black stars), focal mechanisms and proposed fault locations of the 2010 and 2011 Rigan event according to Walker et al. (2013), the IRSC locations of the 2010 and 2011 events (black stars with white outlines), the IRSC location of the 2010 and 2011 event after removal of the geographical bias (white stars), and the positions of the temporary stations (black triangles). (b) Depth distribution of the events, projected along the AA profile shown in (a). Depth scale is in km. No vertical exaggeration is applied for the topography.

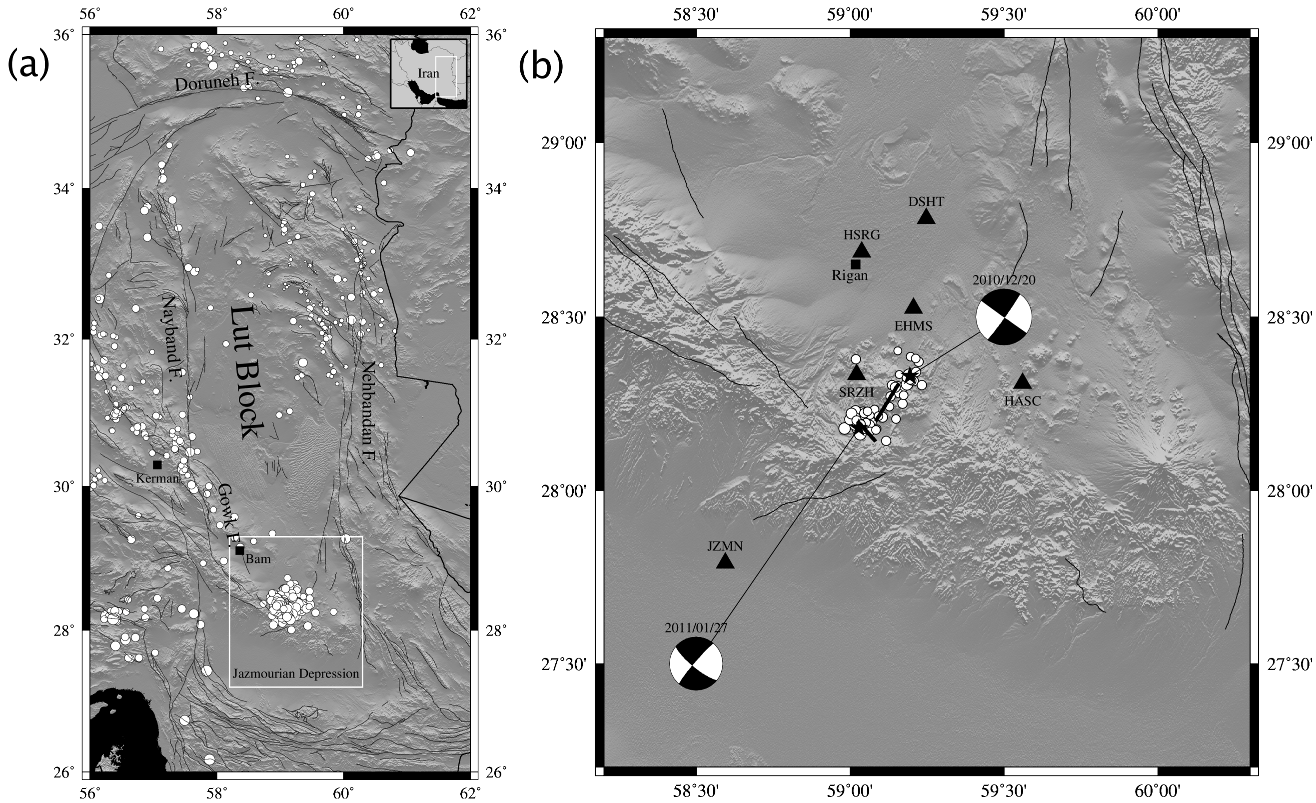

Figure 1. The region of interest for this study. (a) Seismo-tectonic setting of the Lut block in eastern Iran. Thin black lines indicate the major faults. White circles indicate the seismicity of the Lut block (ML 2.5) as recorded by the Iranian Seismological Center (IRSC) during the first three months after the 20 December 2010 event. The white rectangle shows the region of study. (b) Zoom on the region of study showing locations of the aftershocks that were located by Walker et al. (2013). Black stars and thick black lines indicate respectively the epicenters and the fault traces proposed by Walker et al. (2013) for the 20 December 2010 and the 27 January 2011 Rigan events. Their proposed focal mechanisms are also shown. Black triangles indicate the six temporary stations used in this study.

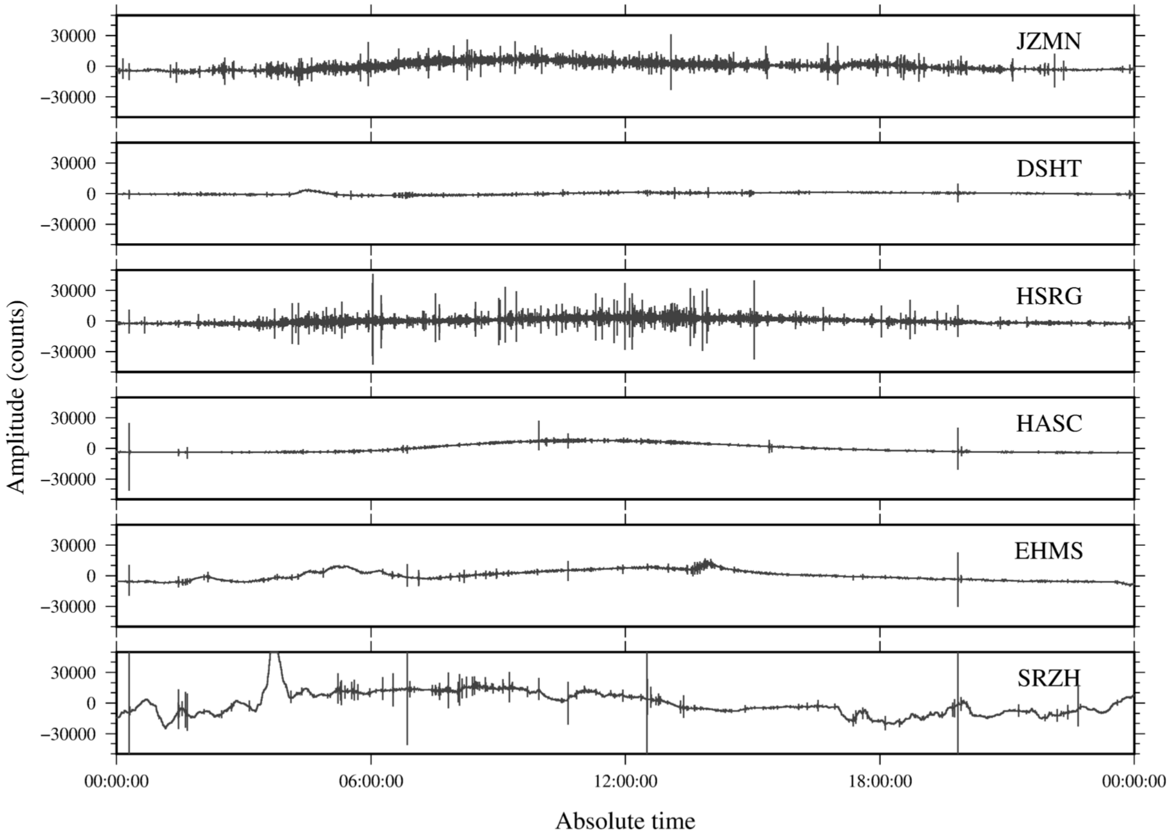

Figure 2. Raw continuous waveforms recorded by the 6 temporary stations in the Rigan region on January 3rd 2011. Station codes are indicated at the right of each waveform. Station locations are shown in Fig. 1b.

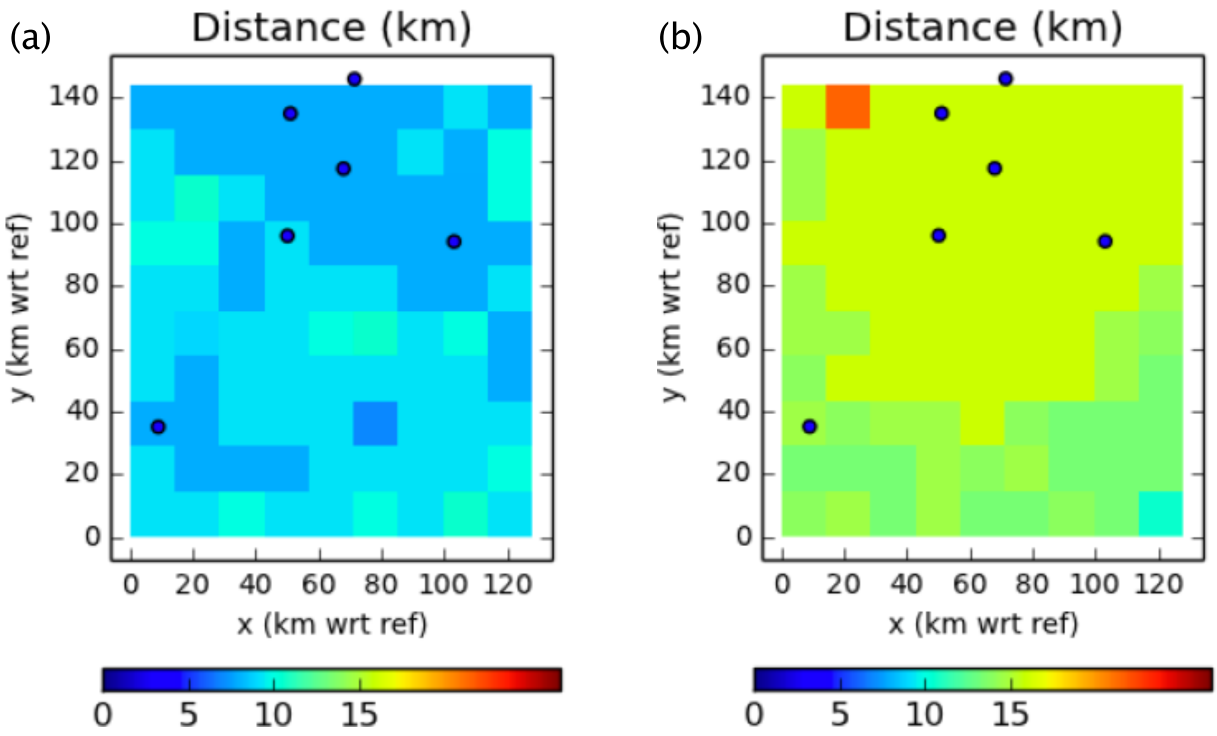

Figure 3. Zero-noise synthetic resolution test for our TR method applied to the Rigan network. Colors indicate the 3D distances between the synthetic input location and the location output by the TR method. Synthetic test-points were placed on a regular grid with 8 km horizontal spacing. (a) Resolution test at 6 km depth. (b) Resolution test at 14 km depth.

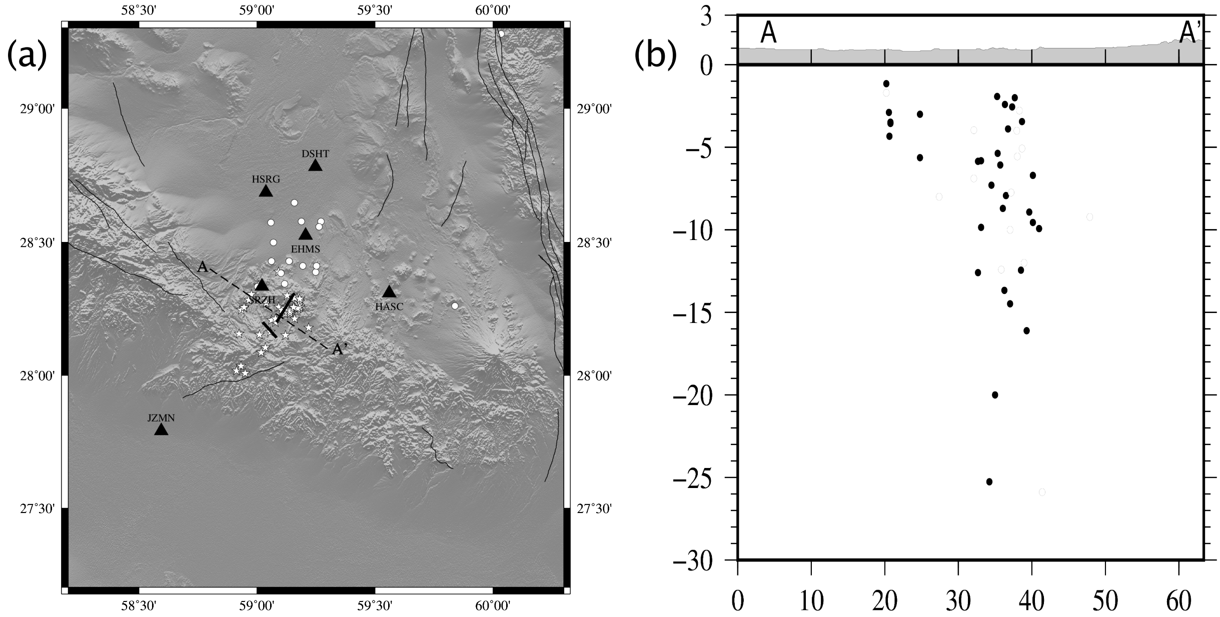

Figure 4. Locations of the 46 well-constrained events obtained using our TR method. (a) Map of the epicenters (white stars), showing also the epicenters of the 14 aftershocks located by IRSC during the time-period we analysed (white circles) and the positions of the temporary stations (black triangles). (b) Depth distribution of the events, projected along the AA profile shown in (a). Depth scale is in km. No vertical exaggeration is applied for the topography.

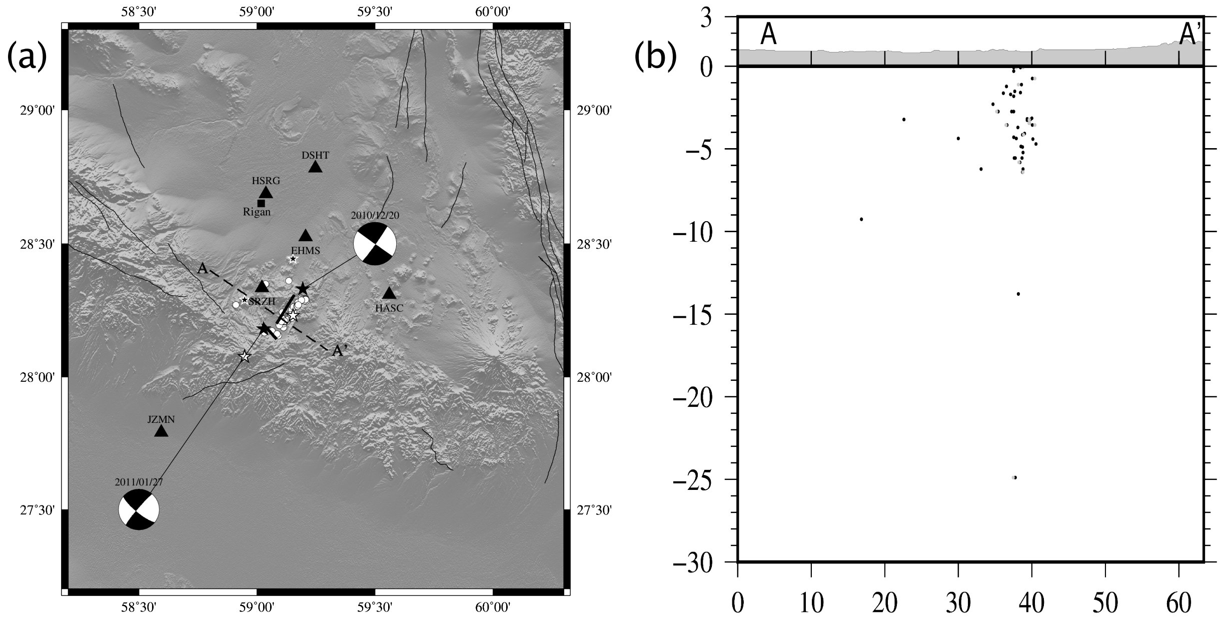

Figure 5. Locations of the 46 well-constrained events obtained using manual picking and NLL. (a) Map of the 46 aftershock epicenters (white circles), showing also the epicenters (black stars), focal mechanisms and proposed fault locations of the 2010 and 2011 Rigan event according to Walker et al. (2013), the IRSC locations of the 2010 and 2011 events (black stars with white outlines), the IRSC location of the 2010 and 2011 event after removal of the geographical bias (white stars), and the positions of the temporary stations (black triangles). (b) Depth distribution of the events, projected along the AA profile shown in (a). Depth scale is in km. No vertical exaggeration is applied for the topography.